Physical models for rock engineering

Author: Prof. Dr. habil. Heinz Konietzky
(TU Bergakademie Freiberg, Geotechnical Institute)

Editor: Prof. Dr.-Ing. habil. Heinz Konietzky Layout: Gunther Lüttschwager
TU Bergakademie Freiberg, Institut für Geotechnik, Gustav-Zeuner-Straße 1, 09599 Freiberg • sekr_fm@ifgt.tu-freiberg.de

1 Introduction

Physical modelling is a widespread technique to investigate the behaviour of constructions at a reduced scale. A comprehensive review about the use of scaled models in civil engineering is provided by Lirola et al. (2017). Physical modelling in geotechnical engineering is a traditional technique to investigate the behaviour of geotechnical constructions and natural geological objects (e.g. slopes, faults, caves etc.) under complex loading conditions incl. coupled hydro-thermal-mechanical-chemical ones. The loading can be highly dynamic (e.g. earthquake or impact loading) or long-term for instance creep or swelling phenomena. The main characteristic of physical modelling is that the object under investigation in nature is duplicated by a small-scale lab model with a certain scale (small scale prototype).

Compared to other investigation tools, physical modelling has the advantage, that it can duplicate very complex conditions in terms of shape, material behaviour, loading etc. Physical models also provide excellent conditions to perform measurements and monitoring and to control the test conditions (e.g. temperature, humidity, loading conditions etc.). The disadvantage is, that set-up of such models is very time consuming and costly. Also, failure states can be observed only ones, because the model will be destroyed during the experiment.

Generally, physical modelling is based on two fundamental theories:

- similarity theory
- dimensional analysis

Based on these theories, materials and corresponding properties, applied loads, the method of model construction, boundary conditions, measurements, monitoring etc. have to be chosen and adopted, respectively.

According to 1 g physical models (models under natural gravity), two approaches can be distinguished (Bakhtar, 2000):

- material scaling: geometry (size), strength and loads are scaled
- replica scaling: geometry is scaled, but strength related properties are not scaled (match original material)

Most physical modelling is performed using material scaling. A comprehensive overview about dimensional analysis and application for design of physical models in rock mechanics is given in Obert & Duval (1967).

2 Scaling

Scaling has to be done in respect to:

- model dimensions (model size)
- material properties
- loads

Physical equivalence is guaranteed by considering the similarity coefficients *SC* (ratio between considered quantity in-situ related to model). The geometrical similarity coefficient SC_L describes the ratio between in-situ dimension and model dimension. Exemplary, the following holds assuming an elasto-plastic Mohr-Coulomb material behaviour:

$$\frac{SC_\sigma}{SC_\gamma \cdot SC_L} = 1, \quad \frac{SC_U}{SC_\varepsilon \cdot SC_L} = 1, \quad \frac{SC_\sigma}{SC_\varepsilon \cdot SC_E} = 1, \quad \frac{SC_\sigma}{SC_C} = 1, \quad SC_\varepsilon = SC_\phi = SC_\nu = 1,$$

With:

SC_σ similarity coefficient for stress (load),
SC_ε similarity coefficient for deformation,
SC_ϕ similarity coefficient for friction coefficient,
SC_C similarity coefficient for cohesion,
SC_E similarity coefficient for Young's modulus,
SC_ν similarity coefficient for Poisson's ratio,
SC_γ similarity coefficient for specific gravity,
SC_L similarity coefficient for geometry scale,
SC_U similarity coefficient for displacement,

If we have defined a geometrical scale SC_L and we want to adjust stiffness and strength of the materials used for the physical model, the following equations should be applied (subscript 'm' represents the model):

$$\nu_{\text{m}} = \nu_{\text{in-situ}} \qquad \phi_{\text{m}} = \phi_{\text{in-situ}}$$

$$\frac{\sigma^t_{\text{in-situ}}}{\sigma^t_{\text{m}}} = \frac{\sigma^c_{\text{in-situ}}}{\sigma^t_{\text{m}}} = \frac{c_{\text{in-situ}}}{c_{\text{m}}} = \frac{E_{\text{in-situ}}}{E^t_{\text{m}}} = const. \qquad \frac{F_{in-situ}}{F_{\text{m}}} = \frac{E_{in-situ}}{E^t_{\text{m}}} \cdot SC_L^2$$

where: *F*: applied force, *E*: Young's Modul, σ^t: tensile strength, σ^C: compressive strength, ν = Poisson`s ratio, Φ = friction angle and c = cohesion.

The scale values for force SC_F as well as for stress and Young's modulus are:

$$SC_\sigma = SC_E = SC_L \cdot SC_\gamma \qquad SC_F = SC_\gamma \cdot SC_L^3$$

If we assume a model with length scale of 1:50 and a specific gravity scale of 1:2 we obtain a force scale of 4e-6 and a stress scale of 1e-2.

Tab. 2.1: Scale factors for mechanical properties (Bakhtar, 2000)

Quantity	Dimensional form	Scale factor^{+}
Linear dimension	L	l^*
Area	L^2	l^{*2}
Volume	L^3	l^{*3}
Density	ML^{-3}	$m^* l^{*-3}$
Time	T	$l^{*1/2}$
Stress	$ML^{-1}MT^{-2}$	$m^* l^{*-2} = m^* l^{*-1} t^{*-2}$
Force	$MLMT^{-2}$	$m^* l^* t^{*-2} = m^*$
Velocity	LT^{-1}	$l^{*1/2}$
Acceleration	LT^{-2}	$l^* t^{*-2} = 1$
Angular velocity	T^{-1}	t^{*-1}
Mass	M	$M^* = \rho^* l^{*3}$
Energy	ML^2T^{-2}	$m^* l^{*2} t^{*-2}$
Impulse	MLT^{-1}	$m^* l^* t^{*-1}$
Strain	LL^{-1}	1
Friction angle	L^0	1
Poisson's ratio	$\Delta l_1/L_1/\Delta l_2/L_2$	1
Frequency	T^{-1}	t^{*-1}
Curvature	L^1	l^{*-1}

Bakhtar (2000) has summarised some mechanical scaling factors (see Tab. 1.1) based on the basic quantities mass (*m*, *M*), length (*l*, *L*) and time (*t*, *T*). Derived quantities are then for instance: force (MLT^{-2}) or velocity (LT^{-1}). The relations become more complex in case of non-linear behaviour of the material. Bakhtar (2000) describes how dynamic processes can be scaled.

Dependent on the problem of investigation, besides the geometrical similarity, also kinematic (similarity of motion) and dynamic similarity (similarity of forces) should be considered. The general theoretical concept of physical models is based on Buckingham's π-Theorem and dimensional homogeneity of the corresponding equations (see for instance Hutter et al. (2014) or Gibbings (2011).

Qiu et al. (2021) describe a physical model to investigate the blasting effect and give details about scaling of dynamic parameters. Li et al. (2020) describe scaling relations for hydro-mechanical coupled physical models. Ning et al. (2025) provide an up-to-date overview about physical model technology for underground structures.

Tab. 2.2: Similarity scaling for natural earth gravity and model under specific gravity *n* (Ning et al. 2025)

Physical quantity		Relationship of similar constants	Scope of application	
			Model in normal gravity environment	Model in hypergravity environment
L	Size	$C_L = \frac{L_p}{L_m}$	λ	λ
g	Gravity	$C_g = \frac{g_p}{g_m}$	1	$n(n \neq 1)$
ρ	Density	$C_\rho = \frac{\rho_p}{\rho_m}$	a	a
r	Unit weight	$C_r = C_\rho C_g$	a	na
t	Time	$C_t = \sqrt{\frac{C_L}{C_g}}$	$\sqrt{\lambda}$	$\sqrt{\frac{\lambda}{n}}$
ε	Positive strain	$C_\varepsilon = 1$	1	1
υ	Poisson's ratio	$C_\upsilon = 1$	1	1
ϕ	Internal friction angle	$C_\phi = 1$	1	1
μ	friction coefficient	$C_\mu = 1$	1	1
γ	Shear strain	$C_\gamma = 1$	1	1
e	Volume strain	$C_e = 1$	1	1
σ	Positive strain	$C_\sigma = C_L C_r$	$a\lambda$	$na\lambda$
s	Displacement	$C_s = C_L C_\varepsilon$	λ	λ
E	Elastic modulus	$C_E = \frac{C_\sigma}{C_\varepsilon}$	$a\lambda$	$na\lambda$
G	shear modulus	$C_\tau = C_\gamma C_G$	$a\lambda$	$na\lambda$
τ	Shear stress		$a\lambda$	$na\lambda$
R_c	Uniaxial compressive strength	$C_{R_c} = C_\sigma$	$a\lambda$	$na\lambda$
R_τ	Shear strength	$C_{R_\tau} = C_\tau$	$a\lambda$	$na\lambda$
c	Cohesion	$C_c = C_\sigma$	$a\lambda$	$na\lambda$

3 Measurements

In principle all usual lab-based measurement techniques can be used to monitor the behaviour of a physical model. Therefore of course, the measurement scheme strongly depends on the problem under investigation. Nevertheless, a few methods are particular important (see also Figures 3.1 to 3.3):

- High-speed cameras
- Optical deformation measurements (e.g. digital image correlation, fibre optics)
- Observation of markers placed at specific points or selected profiles (displacements, rotations)
- Monitoring via specific locally placed sensors (e.g. mechanical pressure, water pressure, temperature, fluid flow velocity etc.)
- Continuous monitoring of any kind of applied loading

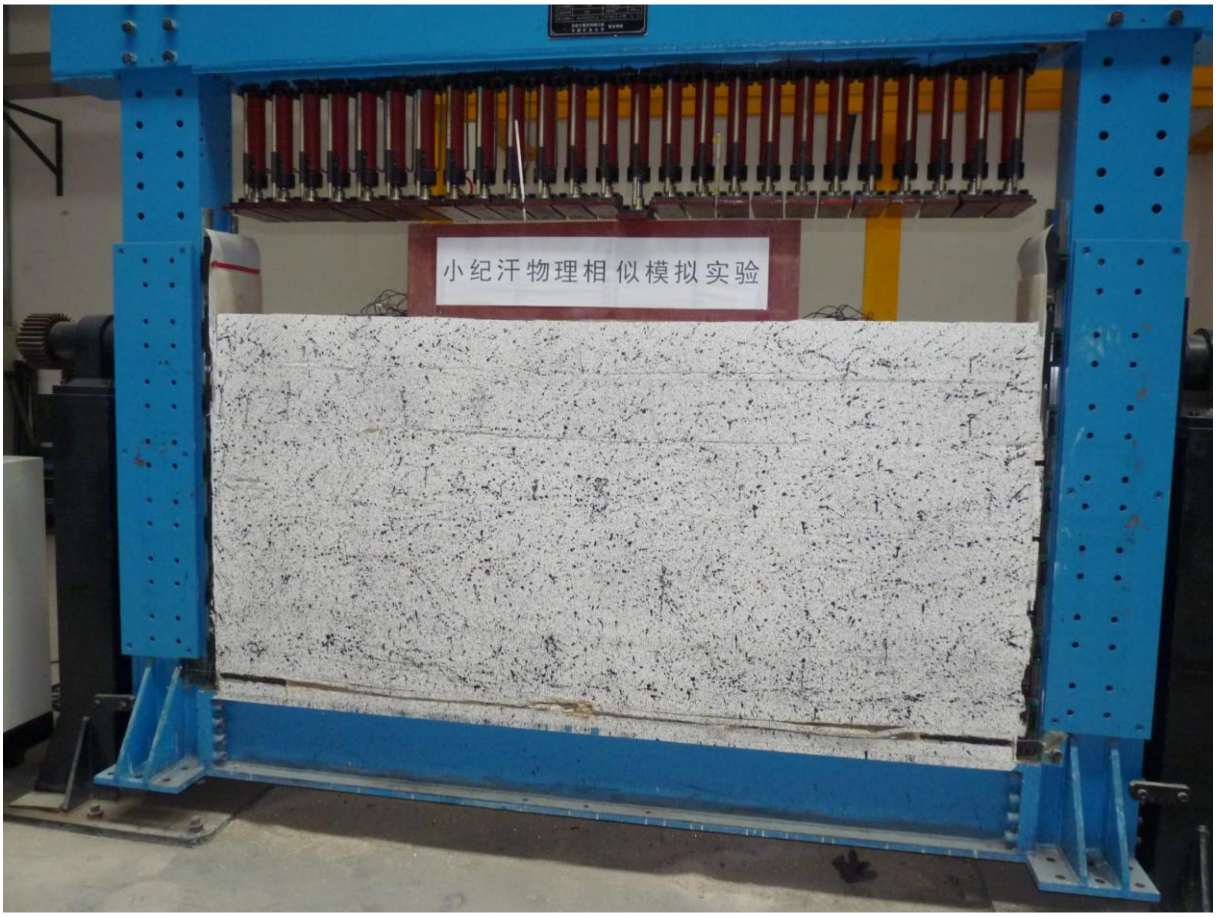

Fig. 3.1: Physical model prepared for image correlation via sprayed surface (China)

Fig. 3.2: Physical model prepared with point markers to monitor movements (China)

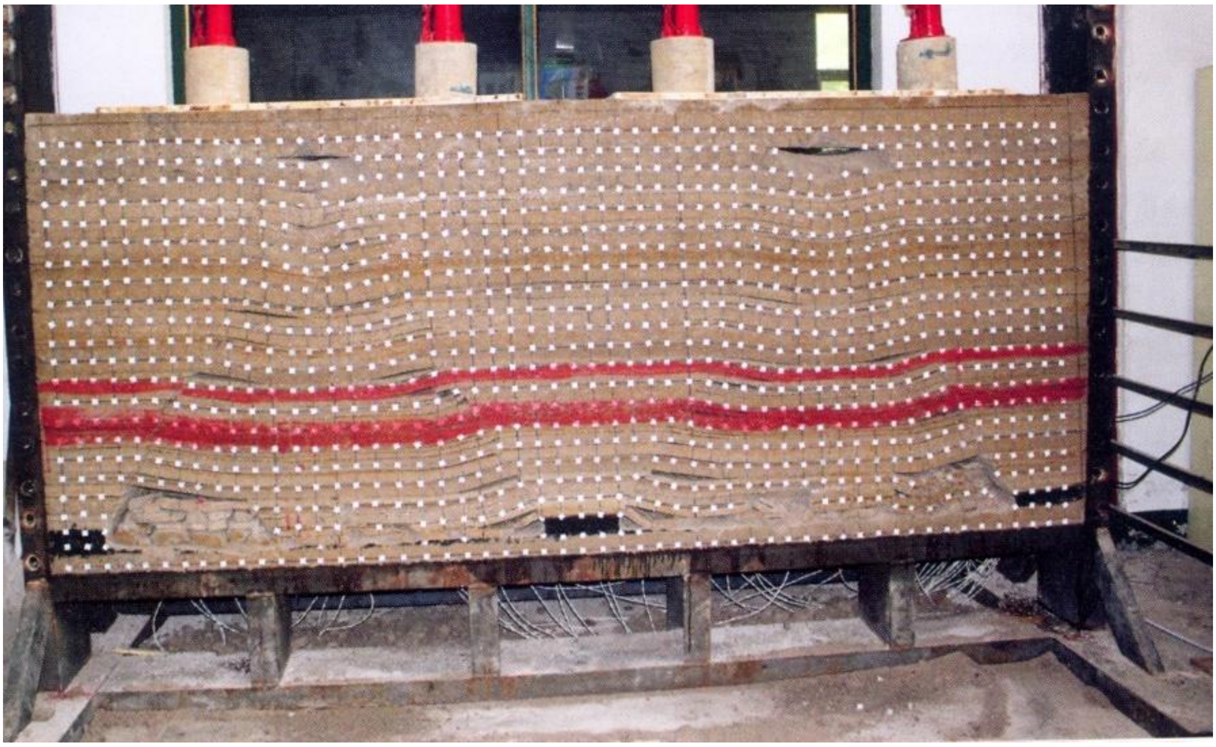

Fig. 3.3: Physical model prepared with point and profile markers to monitor movements (China)

4 Materials

The choice of materials used to construct physical models depends mainly on the specific task, model size and available loading magnitudes. Typical materials used for simulating rocks are:

- Different types of concrete
- Different types of plaster
- Materials available for 3D-printers (different plastics etc.; e.g. Song et al. 2018)
- Specific glues with different aggregates
- Special ceramics
- Weak natural rock materials
- Specific materials to represent specific construction components (e.g. special metals do represent anchors)

An overview for equivalent materials for soft rocks is given by Mei et al. (2017). Geological layering, faults, inclusions etc. can be simulated by materials with different properties like illustrated in Fig. 4.1 for a tunnel in a slightly inclined layered rock mass (sequence of coal bearing layers and sandstone / silt layers).

Fig. 4.1: Physical model with inclined layering representing strata with different properties (China)

Tab. 4.1: Examples for similar materials (Ning et al., 2025)

Objects	Raw materials	Curing principle	Characteristics	Application
Engineering geomechanics model material	PbO/Pb_3O_4, gypsum, bentonite	Inorganic cementation	High unit weight, low elastic modulus, low strength, expensive and toxic	–
MIB and MSB geomechanics model materials	Aggregates: iron powder, barite powder, red lead powder. Binders: rosin alcohol solution, paraffin. Additive: chloroprene	Physical compaction, organic cementation	High unit weight, low elastic modulus, low strength, near natural rock shear strength, slightly toxic	Geomechanical model test of caverns in large underground hydropower station
NIOS model material	Aggregates: Fe_3O_4, river sand. Binder: gypsum	Physical compaction, inorganic cementation	High unit weight, stable performance, no toxicity, no dust, cheap, convenient preparation, environmental friendliness	Model test of powerhouse cavern group in underground hydropower station
Solid-fluid coupling similar material	Aggregate: sand. Binder: paraffin	Physical compaction, organic cementation	Good non-hydrophilicity	Model test of coal seam longwall mining overlain by water-rich wind-blown sand layer
Brittle rockburst similar material	Aggregate: quartz sand. Binders: gypsum, cement. Humectant: glycerol. Retarder: gelatin	Inorganic cementation	Rockburst characterisitics like hard brittle rock	Rockburst model test of brittle hard rock
Cementitious geotechnical similar material for iron crystal sand	Aggregates: fine iron powder, barite powder, quartz sand. Binder: rosin alcohol solution. Additive: gypsum	Physical compaction, organic cementation	Wide range of mechanical parameters, stable performance, low price, rapid drying, simple process, non-toxic and harmless	Model tests of traffic tunnel, powerhouse, underground storage, mining roadway and other hard rock engineering
Temperature analogous model material	Weighting agent: barite powder. Binder: engine oil. Others: fusible polymer materials and some additives, temperature control system	Molten sintering	The mechanical parameters such as shear strength, cohesion and friction coefficient decrease with the increase of temperature	3-D geomechanical model test on abutment stability of high arch dam in large hydropower station
ETH analogue material for rock	Bassendean sand, white portland cement, water	Physical compaction, inorganic cementation	Suitable uniaxial compressive strength, high maximum internal friction angle, low cohesion, obvious brittleness	Centrifugal simulation test of huge rock flow
Creep similar material of salt rock	Aggregates: industrial salt particle, fine salt powder. Additive: fine iron powder. Binders: epoxy resin, ethylenediamine	Physical compaction, organic cementation	Creep memory properties like salt rock	Model test of Jintan salt rock underground storage
SCVO fluid–solid similar material	Aggregates: sand, barite powder, talc powder. Binders: cement, vaseline. Additive: silicone oil	Physical compaction, inorganic cementation	Good deformation characteristics and hydrophysical properties with flexible forward and reverse adjustment	Moder test of Qingdao Kiaochow Bay tunnel.
Small blocks masonry material	Aggregate: barite powder. Additive: bentonite. Binder: glue (polyvinyl alcohol and water)	Organic cementation	Cheap, suitable for simulating brittle materials such as concrete and rock	Failure model test of Xiluodu arch dam
Similar material for weak surrounding rock mass of class IV	Barite powder, quartz sand, gypsum, laundry liquid, water	Physical compaction, inorganic cementation	The material ratio can be adjusted to simulate surrounding rock of different strength	Model test of tunnel surrounding rock mass stability
3D printed photopolymeric material	Photosensitive materials: Vero Clear, Vero White Plus, Fullcure 705	Ultraviolet curing	Good photoelastic properties, internal structure visualization	Model test of natural coal rock with complex fracture
Similar material for methane-bearing coal	Aggregate: coal powder. Binder: sodium humate aqueous solution	Physical compaction	The weight, porosity and adsorbability are close to those of raw coal. Cheap, non-toxic and stable performance	Coal and Gas outburst simulation test
3D printed gypsum-based material	Gypsum powder, binder	Organic cementation	Compressive deformation and failure properties similar to those of rock, but the brittle fracture properties are poor	Test on specimens containing prefabricated crack and lining support tunnel model
Transparent rock mass similar material	Silica powders, liquefied paraffin wax and tridecane	Physical compaction, organic cementation	Good transparency and mechanical characteristics similar to soft rock	Model loading test of soft rock similar
Fracture network model material	Polylactate (PLA)	Molten sintering	3D printing materials with environmental friendliness, strong ductility	Fracture network model of linear and rough jointed rock mass
Fluid-solid coupling similar-material	Aggregates: sand, calcium carbonate, talc powder Binders: white cement, vaseline. Additive: anti-wear hydraulic oil	Physical compaction, inorganic cementation	Good hydrophilicity, compressive strength, tensile strength, brittleness and permeability coefficient	Model test of water inrush from coal seam floor
Surrounding rock material for simulating coal seam mining	Sand, gypsum, calcium carbonate, water	Physical compaction, inorganic cementation	The material strength is controlled by adjusting the ratio of gypsum and calcium carbonate to simulate soft or hard rock strata	Model test of underground coal seam mining
Marl similar material	Aggregate: river sand. Binders: cement, gypsum. Additives: diatomaceous silica, red clay, marlstone powder	Physical compaction, inorganic cementation	The raw rock properties with different weathering degrees can be simulated by adjusting the material ratio and adding different additives	Geomechanical model test of weathered marl
Rock-like material with ultra-low permeability and air tightness	Aggregates: fine iron powder, barite powder, quartz sand. Binder: special cement. Additives: cement, starch	Physical compaction, inorganic cementation	Ultra-low permeability and air tightness, adjustable parameters, easy molding	Gas-solid coupling model tests such as coal and gas outburst, shale gas extraction
3D printed thinly layered rock	Aggregates: magnet iron powder, quartz powder. Binders: cement, gypsum. Others: water, water-retaining agent, retarder	Inorganic cementation	Adjustment of material properties by adjusting the additive ratio	Mechanical characteristics tests of thinly layered rock specimens with different layering and occurrences
3D printed sand-based material	Aggregate: quartz sand. Binder: furan resin. Additive: benzoic acid	Organic cementation	Good brittleness, low strength, and good mechanical regulability, suitable for simulating brittle hard rock	Comparison of uniaxial loading tests in rock mass models containing a pre-existing fracture

5 Load equipment

We can distinguish mechanical, hydraulic and thermal loading. Most important is mechanical loading. Most popular are large stiff loading frames in combination with hydraulic props. They can produce uniaxial or biaxial loading under approximate plane stress conditions (see Fig. 5.1). In addition, but very rare are very large triaxial machines, which can be used also (see Fig. 5.2). Quite flexible and often used in civil engineering are movable wall and frame constructions like shown in Fig. 5.3, where hydraulic props as well as the model itself can be placed in any desired way. In case of dynamic loading so-called shaking tables (see Fig. 5.4) are used. They allow the simulation of complex earthquake loadings.

Fig. 5.1: Different loading frames (China)

Fig. 5.2: Large scale triaxial device for 3.0 m × 3.0 m x 3.5 m model / sample size (Zhengzhou, China)

Fig. 5.3: Flexible wall-frame construction usable for physical model tests (Vietnam)

Fig. 5.4: Shaking tables (left) with scaled skyscraper model (China, right)

6 Examples

6.1 Water dam

Liu et al. (2003) document a physical model test for the Three-Gorge water dam in China. Fig. 6.1.1. shows the model layout, which consists of 4 main components:

- Loading frame
- Model of dam, rock mass and power house
- Hydraulic props to apply loading
- Measurement system (LVDT’s and strain gauges)

Fig. 6.1.2 shows a photo of the physical model and Fig. 6.1.3 illustrates the fracturing observed during the test applying specific loading conditions.

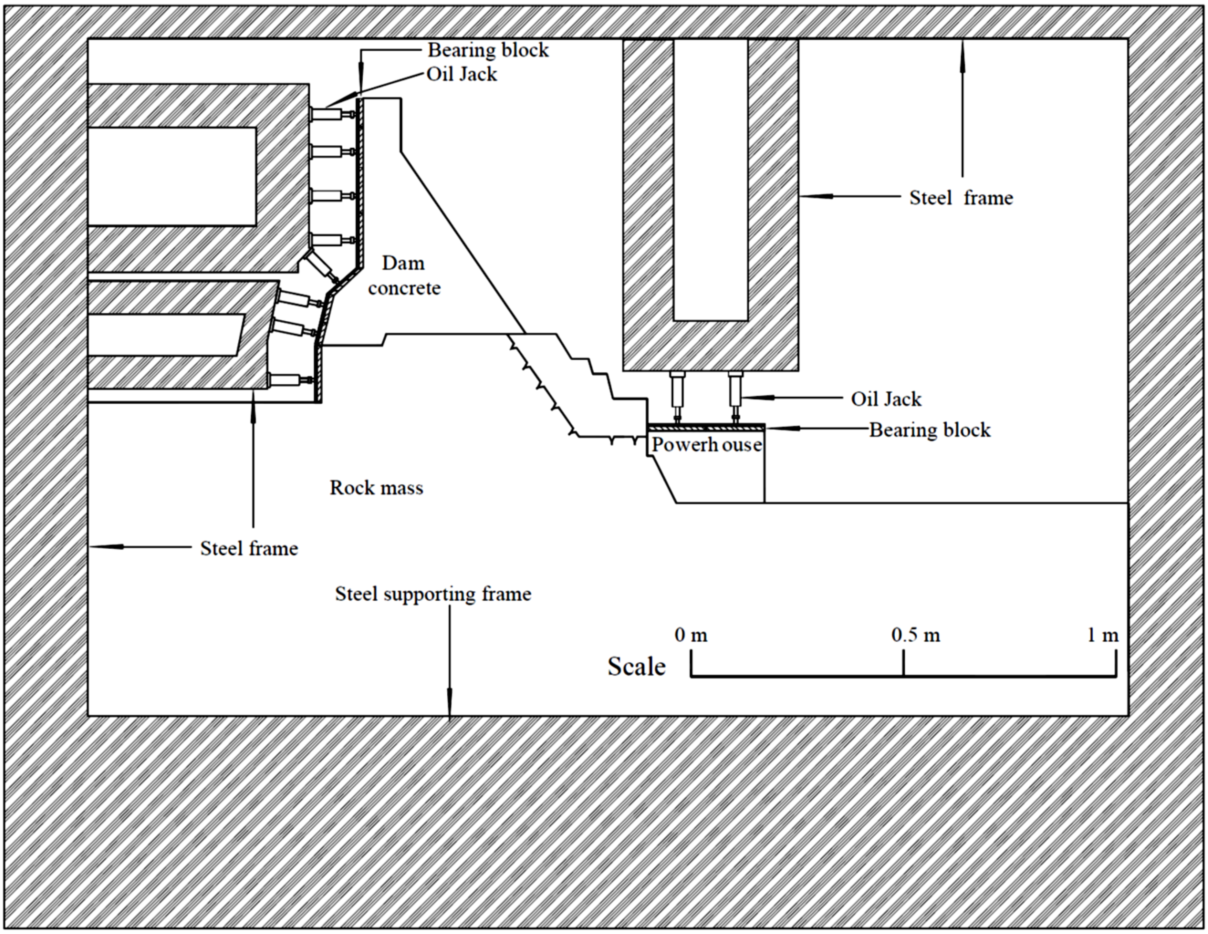

Fig. 6.1.1: Sketch of a physical dam model (Liu et al., 2003)

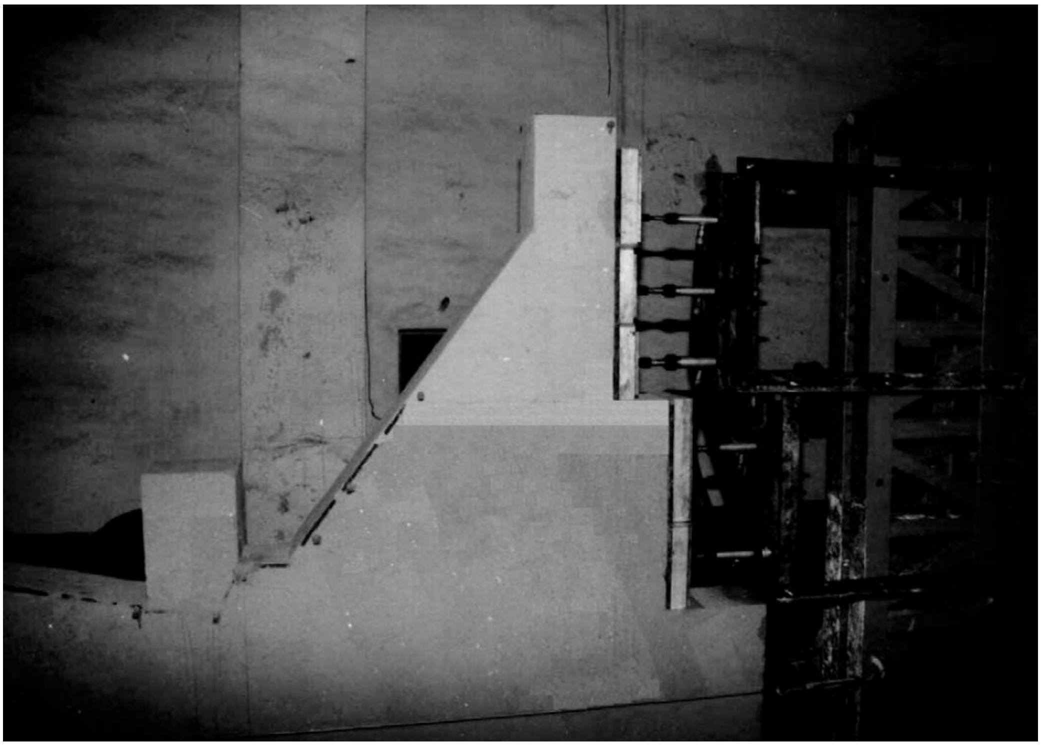

Fig. 6.1.2: Photo of a physical model (Liu et al., 2003)

Tab. 6.1.1 documents the applied scaling values, where:

- C_L: length scaling value
- C_ρ: density scaling value
- C_E: scaling for deformation modulus
- C_σ: scaling for load
- C_c: scaling for cohesion
- C_f: scaling for friction
- C_ε: scaling for strain

Tab. 6.1.2 shows the material parameters for the in-situ material (prototype) and the material used for the physical model.

Tab. 6.1.1: Used scaling values (Liu et al., 2003)

C_L	C_ρ	C_E	C_σ	C_c	C_f	C_ε
120	1.0	120	120	120	1	1

Tab. 6.1.2: Used mechanical properties (Liu et al., 2003)

Mechanical properties	Rock		Dam concrete		Joint		Foundation surface	
	Prototype	Model	Prototype	Model	Prototype	Model	Prototype	Model
Deformation modulus (GPa)	35.0	0.305	26.0	0.21	—	—	—	—
Density (kN/m^3)	27.0	26.8	24.5	24.6	—	—	—	—
Friction angle	59.6°	59.5°	48°	48°	35°	34.2°	48°	45°
Cohesion (MPa)	2.0	0.045	3.0	0.052	0.2	0.0	1.3	0.056

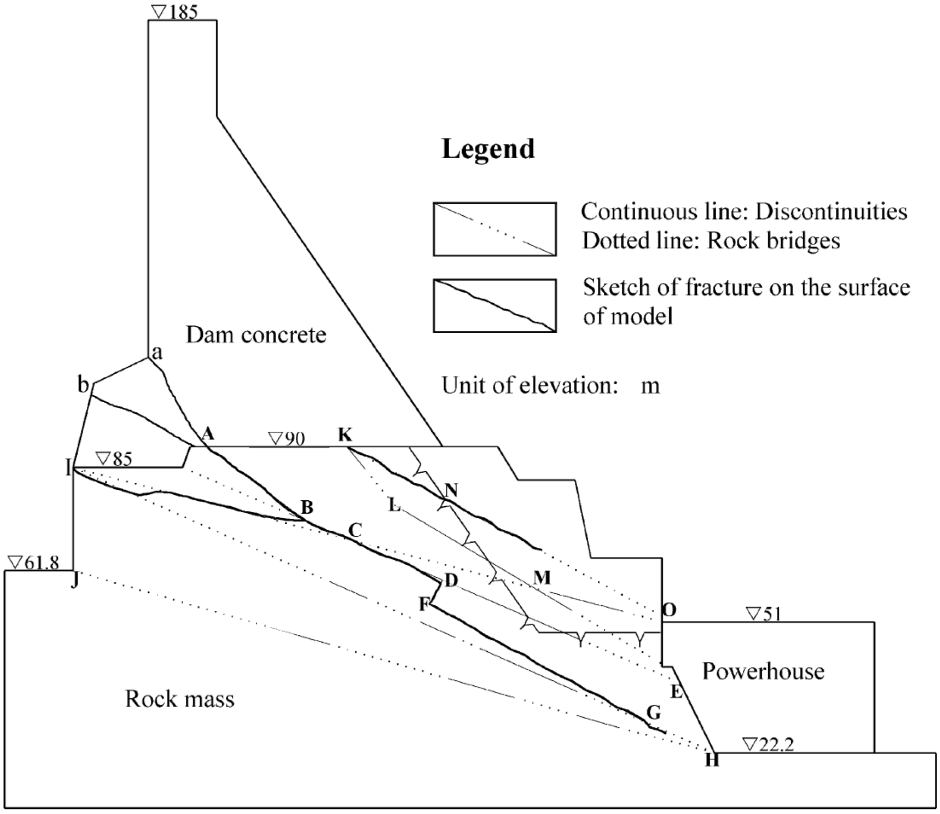

Fig. 6.1.3: Sketch of detected fractures after evaluating physical model (Liu et al., 2003)

6.2 Soil - structure interaction

Al Heib et al. (2013) describe physical model tests to investigate the soil-structure interaction due to ground movements triggered for instance by underground mining, collapse of cavities, swelling etc. The modelled foundation consists of concrete slabs and masonry structures (see Figs 6.2.1 and 6.2.2.). DIC is used as main component for monitoring. Soil is represented by special sand. The induced subsidence is controlled by a hydraulic prop (25 cm × 25 cm cross section) at the bottom centre of the model with a size of 3 m × 2 m × 1 m. Vertical movement of the prop creates a subsidence trough like observed in-situ.

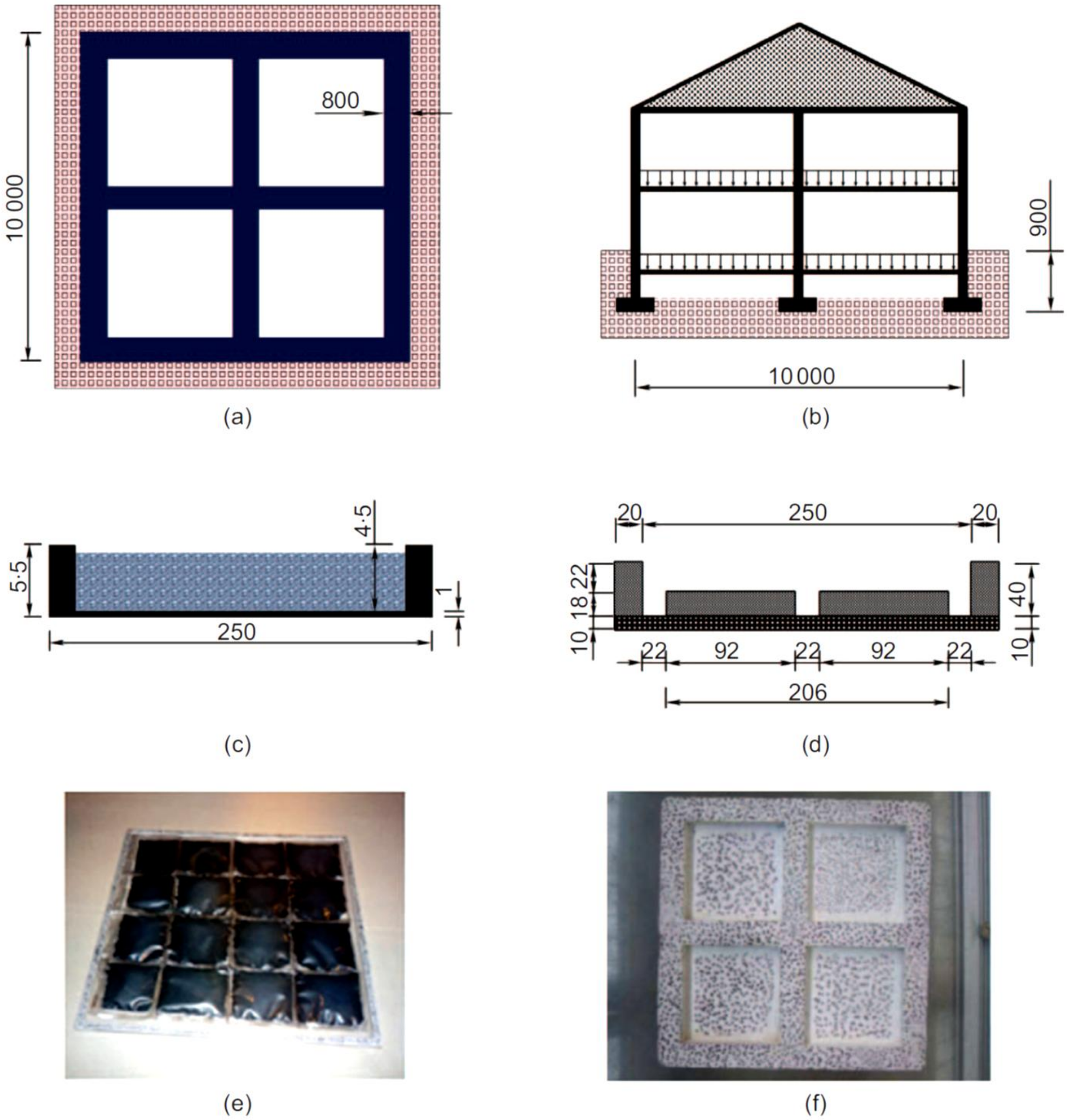

Fig. 6.2.1: Figure to illustrate set-up of physical model: a-b: in-situ situation, c-d: physical model set-up, e-f: pictures (Al Heib et al., 2013)

Tab. 6.2.1: In-situ parameters and scaled parameters for physical model according to Fig. 6.2.1 (Al Heib et al., 2013)

Parameter	Scaling factor	Prototype	Ideal model	Polycarbonate	Silicone
Width: m	40	10	0·25	0·25	0·25
Length: m	40	10	0·25	0·25	0·25
Height: mm	40	250	6·25	4·5	40
Young modulus E: MPa	40	30 000	750	2200–2500	5
Weight: kN	40^3	1000	$15{\cdot}6 \times 10^{-3}$	$15{\cdot}6 \times 10^{-3}$	$21{\cdot}5 \times 10^{-3}$
EA: MN	40^3	$7{\cdot}5 \times 10^4$	1·17	0·75	0·036
EI: N.m^2	40^5	$3{\cdot}9 \times 10^4$	3·81	2·86	3·3
ρ^*	1	$3{\cdot}9 \times 10^{-3}$	$3{\cdot}9 \times 10^{-3}$	$3{\cdot}9 \times 10^{-3}$	$4{\cdot}5 \times 10^{-3}$
α^*	1	2	2	2	0·096

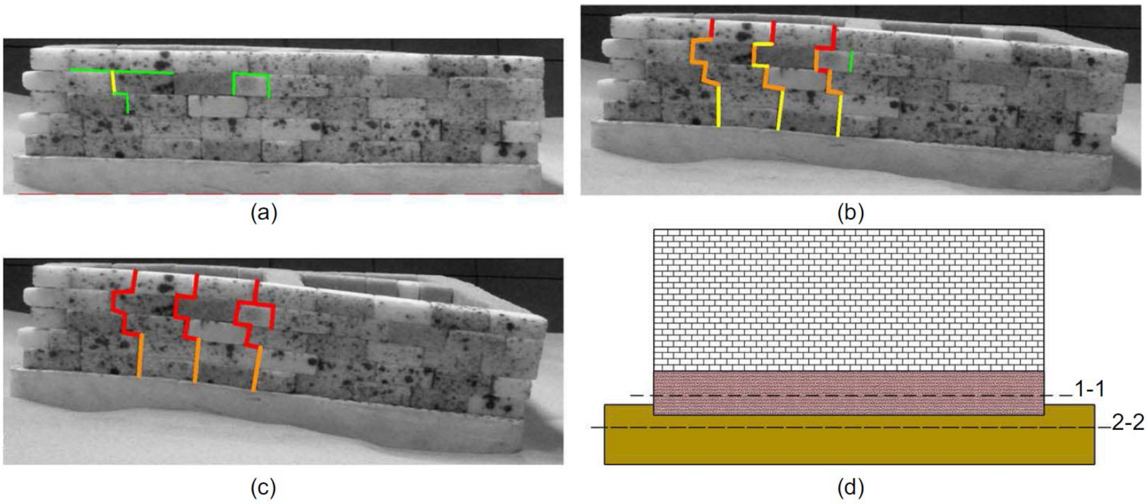

Fig. 6.2.2: Physical model of masonry walls using sugar pieces to represent bricks (Al Heib et al., 2013)

Tab. 6.2.2: In-situ parameters and scaled parameters for physical model according to Fig. 6.2.1 (Al Heib et al., 2013)

Parameter	Prototype blocks	Ideal model	Sugar	Wood
L · l · h: mm	500 × 250 × 200	12·5 × 6·25 × 5	27 × 18 × 12	7 × 7 × 14
Young modulus E: GPa	10 000		Not determined	16 000–19 000
Unit weight: kN/m^3	19·0	19·0	15·90	10·30
Friction angle between blocs φ: °	20–35	20–35	30	30 ± 9

6.3 Underground cavern system

Li et al. (2005) describe a physical model test for an underground cavern system for a hydropower station. Advanced measurement equipment is applied including micro-multi-point extensometers, AE monitoring, optical fiber sensors, internal photography and infrared micro-camera. A micro-TBM is applied to simulate the excavation advance. The chosen geometrical model scale was 1:100. Fig. 6.3.1 shows the underlying project and the corresponding physical model, which represents a part of the whole construction. Fig. 6.3.2 shows the test facility.

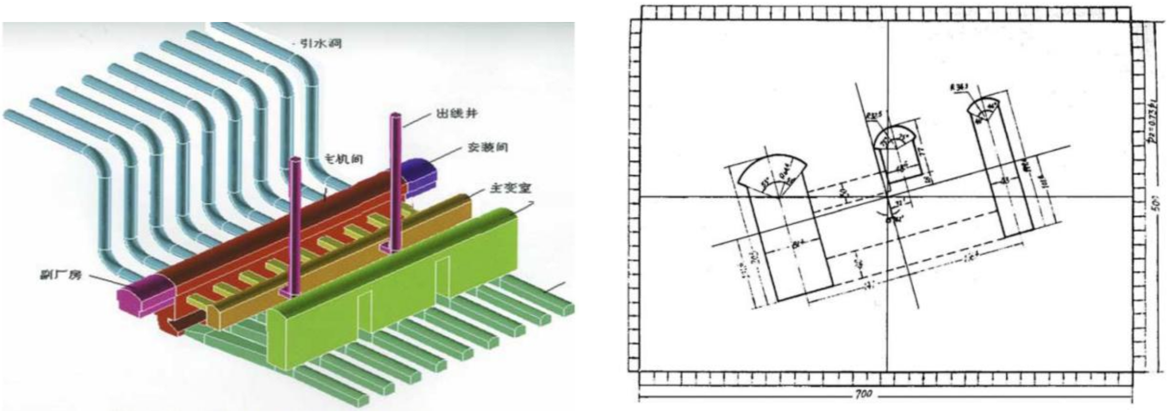

Fig. 6.3.1: Underground cavern system and layout of corresponding physical model (Li et al., 2005)

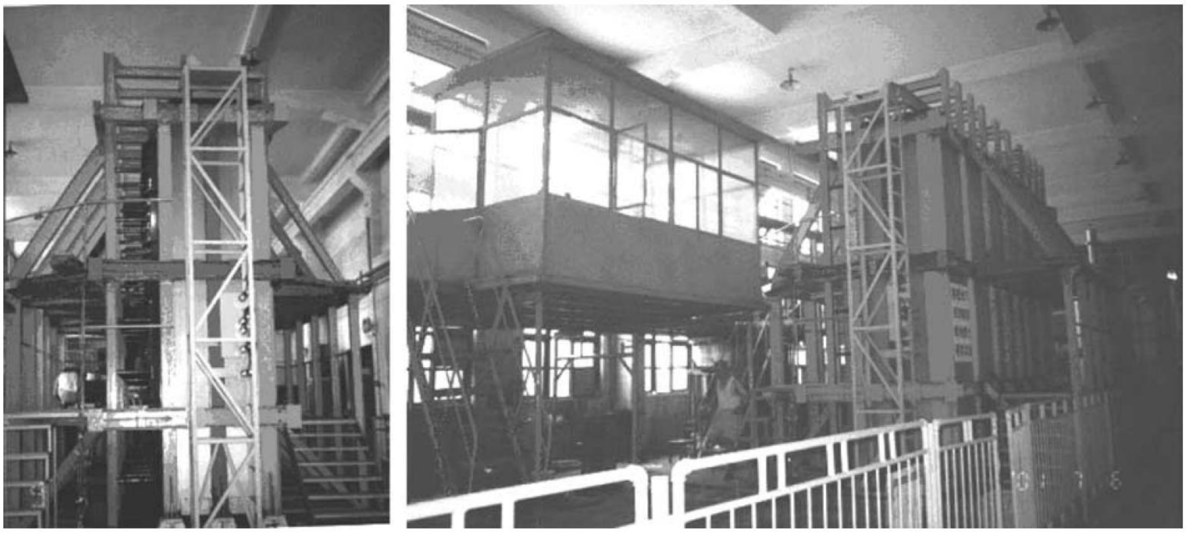

Fig. 6.3.2: Loading frame for large physical model (Li et al., 2005)

6.4 Longwall coal mining

Besides hydropower and dam projects, the physical simulation of longwall coal mining has a longstanding tradition and has reached a quite advanced level in geoengineering. Already Jacobi (1976) has documented very detailed high-level physical modelling results for different elements in longwall coal mining (e.g. supported and unsupported drifts and longwall itself including overlying rock masses). The loading frame for physical longwall tests is 10 m long, 2 m high with a thickness of 0.4 m, the loading frame for physical drift tests is 2 m long, 2 m high with a thickness of 0.4 m (Fig. 6.4.1). The physical models do not only consider the behaviour of the rock mass, but contain also support elements (e.g. anchors, yielding arch support). Therefore, the scaling has to be applied also to the support elements. The typically used length scale *L* was 1:10. This results for instance in the following scaling relations:

- Young's modulus: 1:10
- Poisson's ratio: 1:1
- Frictional coefficient: 1:1
- Density: 1:1
- Compressive strength: 1:10
- Applied forces: 1:1000
- Moment of inertia: 1:10.000 (for structural elements)
- Cross section area: 1:100 (for structural elements)

The applied scaled support measures (see for instance Fig. 6.4.2) were well calibrated in special designed test rigs (see Fig. 6.4.3). Fig. 6.4.4. shows the damage and fracture evolution in the hanging walls as well as the development of the goaf during longwall advance. Fig. 6.4.5. illustrates the deformation and failure pattern of a drift, which is supported with yielding arch support and 2 anchors in the roof. For more recent work see also Cheng et al. (2017) or Zhou et al. (2017).

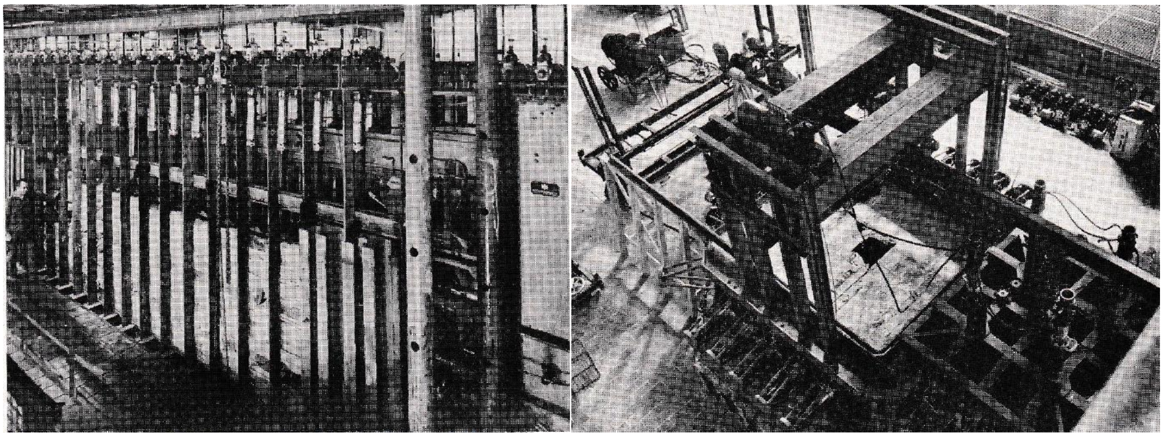

Fig. 6.4.1: Loading frames for longwall (left) and drift (right) physical models (Jacobi, 1976)

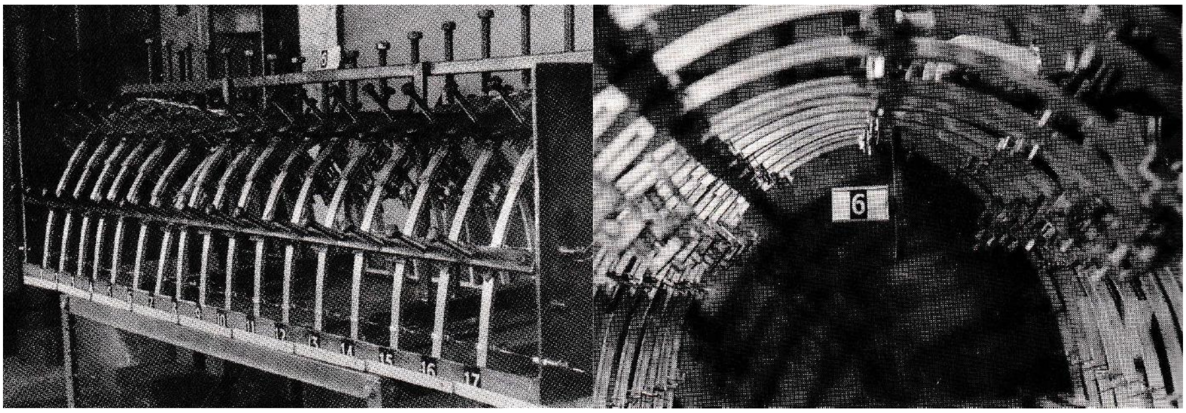

Fig. 6.4.2: Yielding arch support elements prepared for installation inside a physical drift model (Jacobi, 1976)

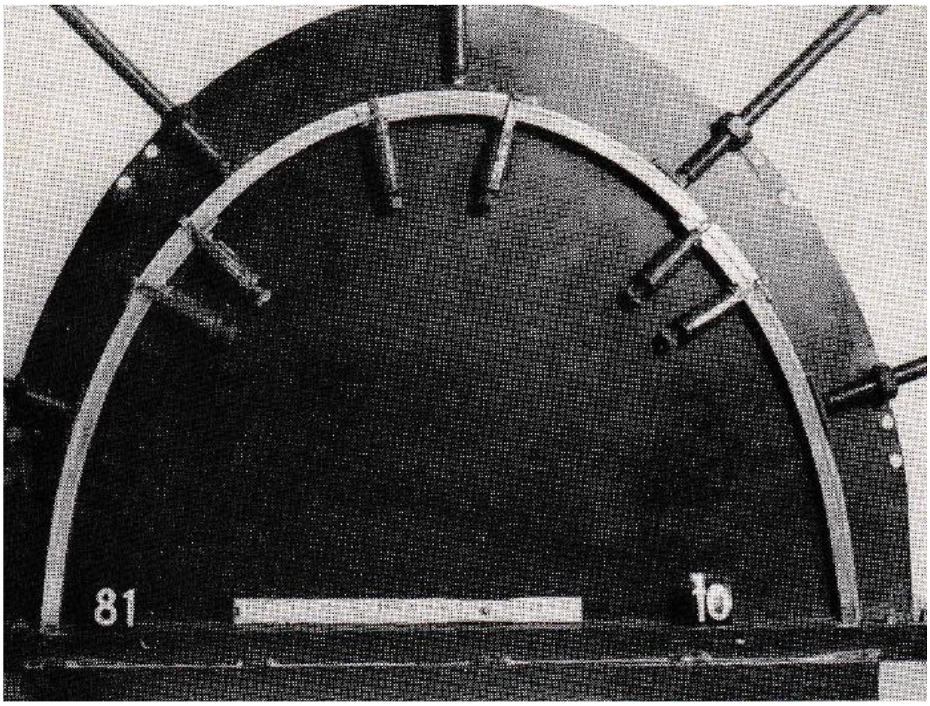

Fig. 6.4.3: Special test rig to calibrate yielding arch support elements for physical drift model with length scale of 1:10 (Jacobi, 1976)

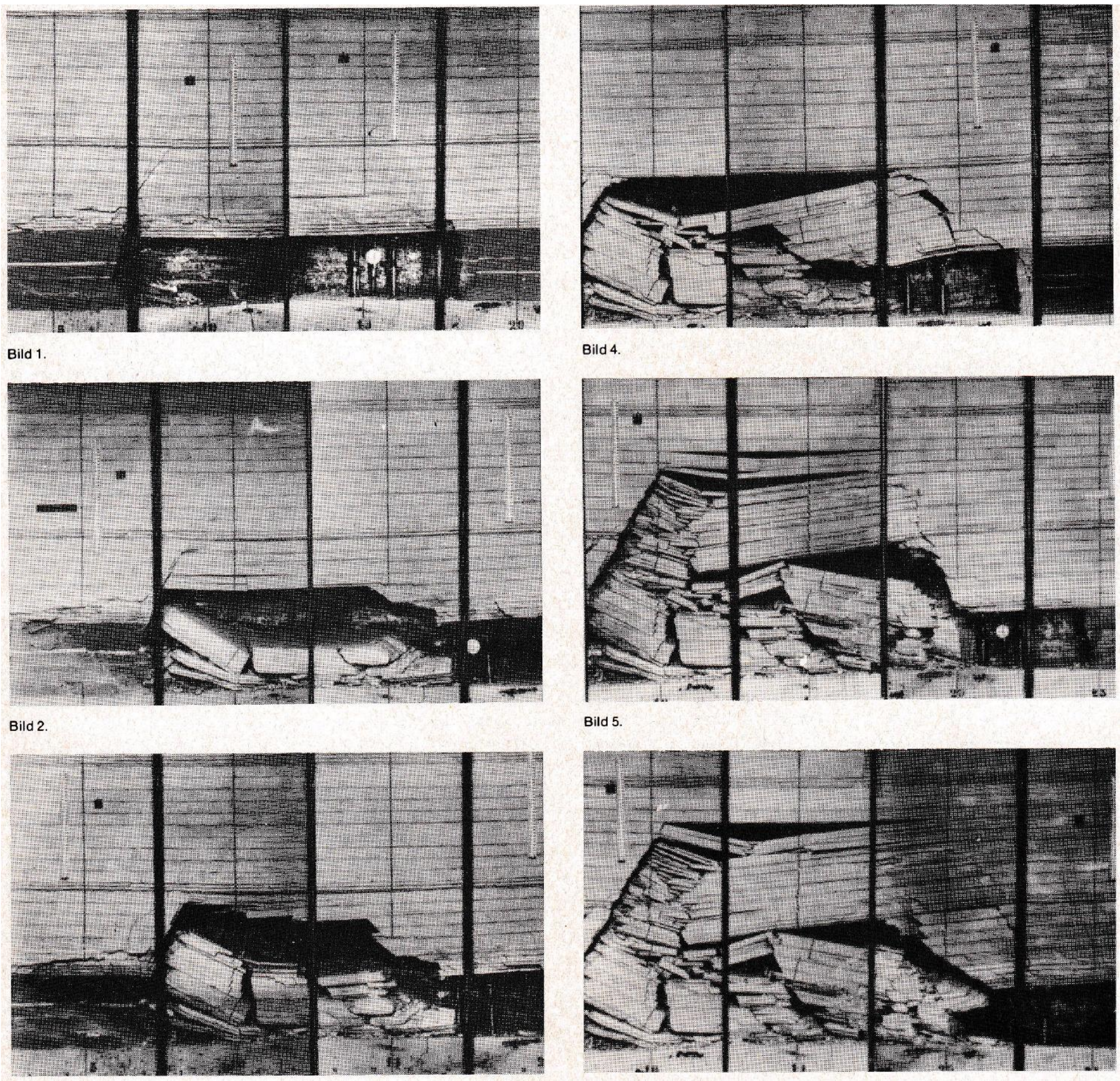

Fig. 6.4.4: Simulation of longwall advance including shield support via physical model: 6 different stages (Jacobi, 1976)

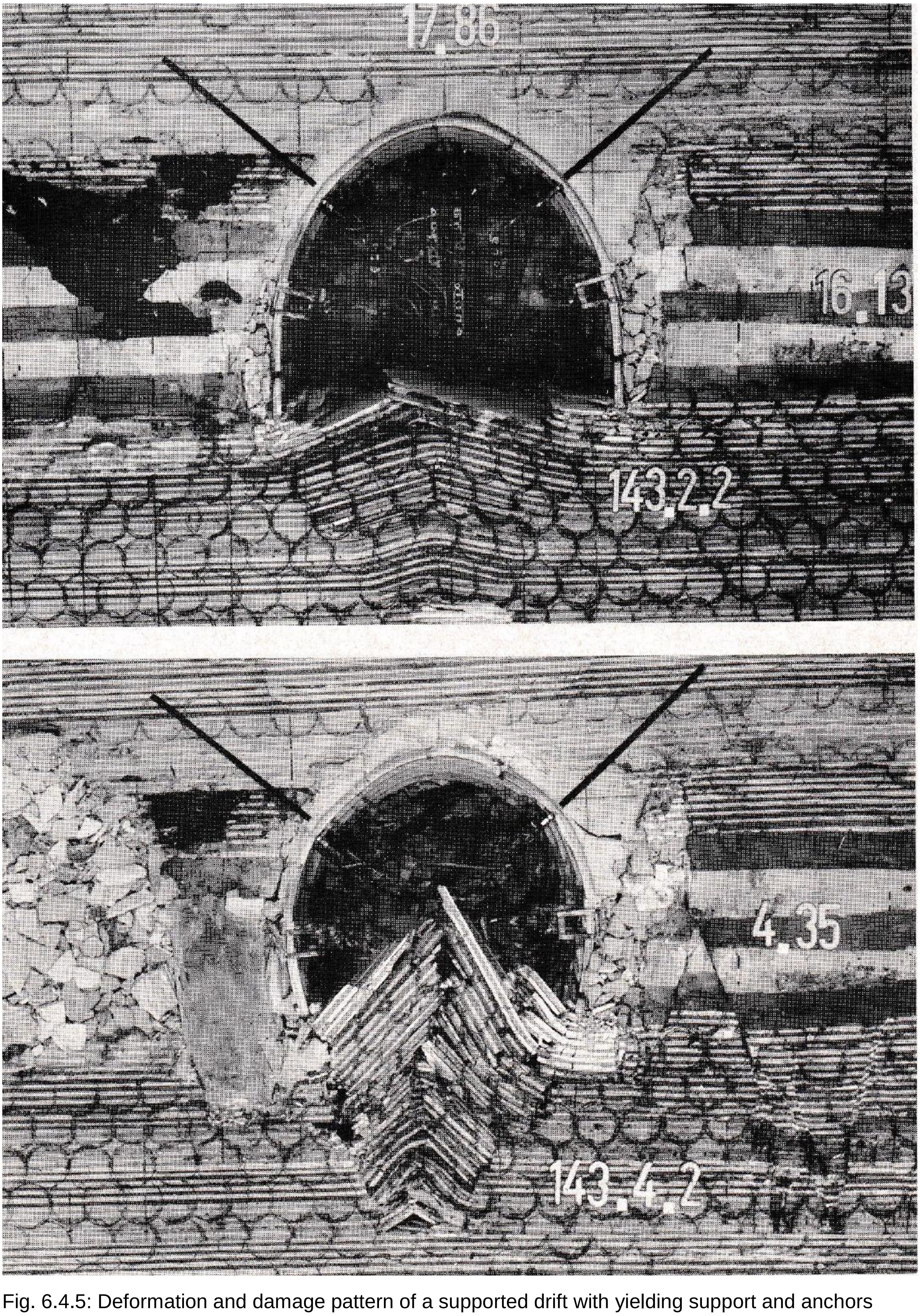

Fig. 6.4.5: Deformation and damage pattern of a supported drift with yielding support and anchors (Jacobi, 1976)

6.5 Sturzstrom simulation

Imre et al. (2010) document dynamical physical modelling using a centrifuge with the aim to investigate the Sturzstrom problem. The aim is to investigate run out, fragmentation and energy balance. The scaling has to consider particle size and size distribution, which should duplicate in-situ values, as well as scaled acceleration inside the centrifuge.

Fig. 6.5.1: Snapshot of high speed camera during test, arrow indicates movement (Imre et al., 2010)

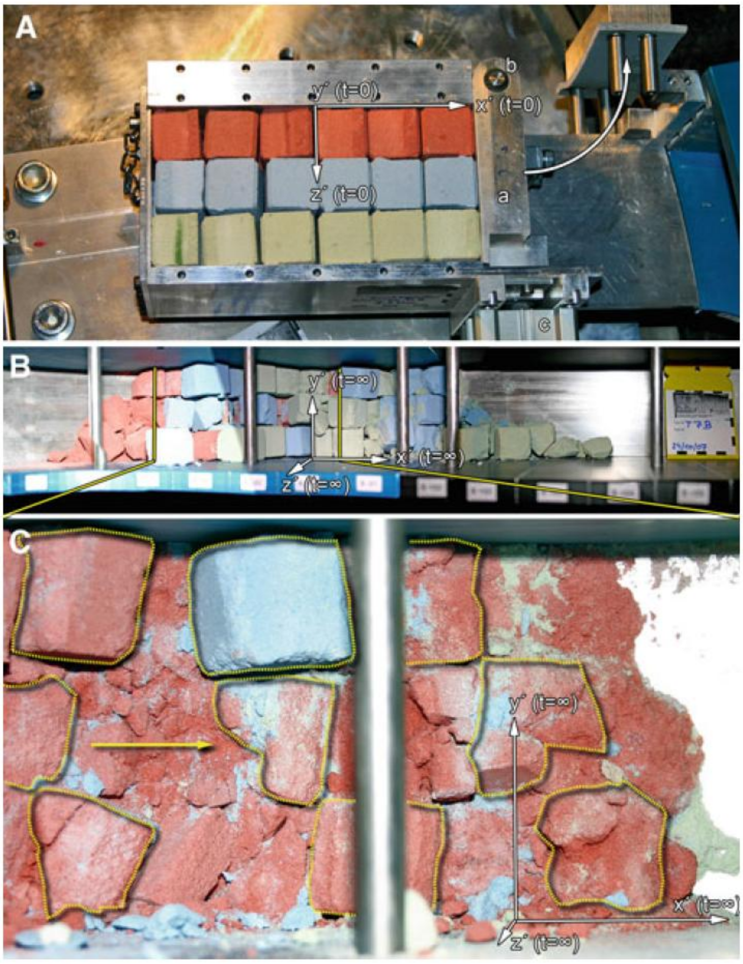

Fig. 6.5.2: Model set-up: (A) hopper section, (B) run out channel, (C) rock flow deposit (Imre et al., 2005)

6.6 *Hydro-mechanical triggered slope failure*

Physical models considering hydro-mechanical coupling are important for slope stability and mass flow problems. For instance, Sharma et al. (2010), Sharma & Konietzky (2011) and Jemai et al. (2017) describe slope failure model tests. High-speed cameras and sensors to measure mechanical and fluid pressure are used. The hydraulic component comprises simulation of rainfall as well as different groundwater levels (see Fig. 6.6.1).

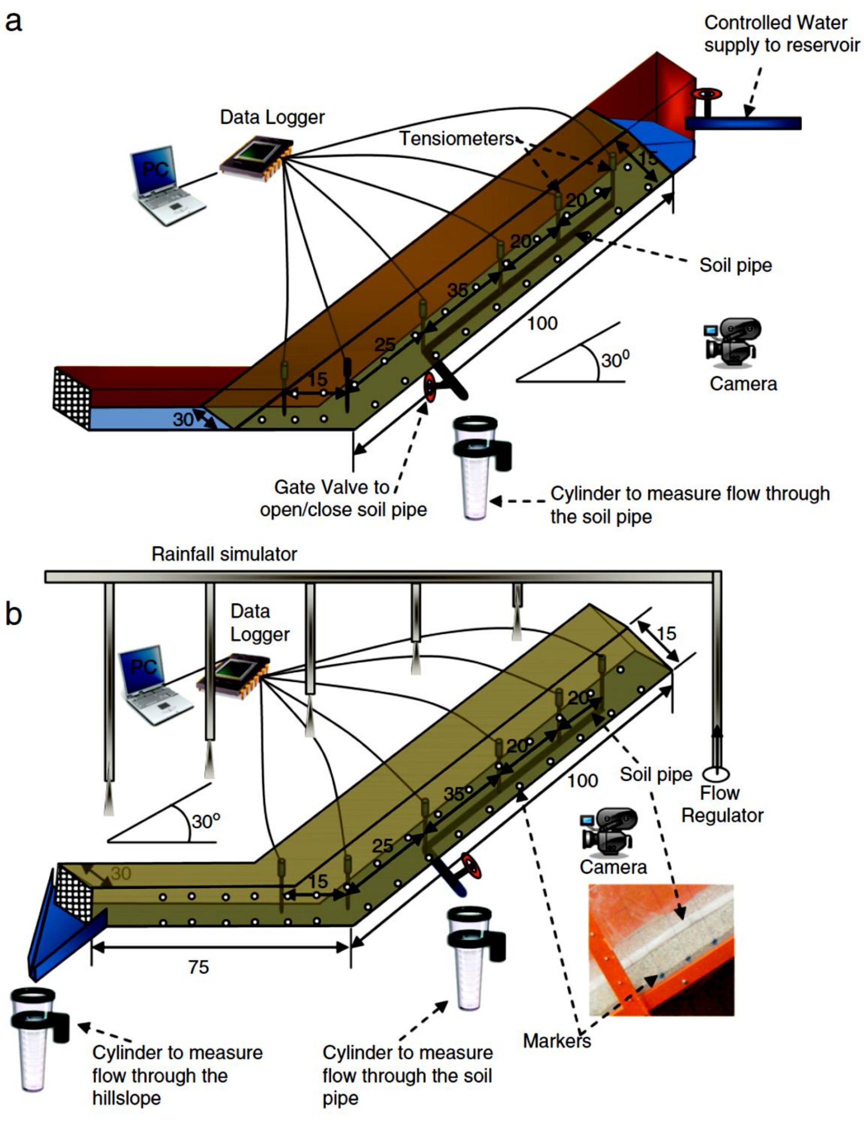

Fig. 6.6.1: Hill slope model to investigate slope failure (Sharma & Konietzky, 2011)

6.7 *Rock slope failure*

Slope instability due to toppling induced by an open-pit mine was investigated by Zhu et al. (2020) using a physical model with size ratio of 1:190. The chosen parameter ratios are: bulk density ratio: 1:1.5; Poisson's ratio and friction angle ratio: 1:1; stresses, deformation modulus, cohesion and total displacements: 1:285 (= 1.5 * 190).

Tab. 6.7.1: In-situ rock mass parameters and corresponding physical model parameters (Zhu et al. 2020)

Lithology	Uniaxial compressive strength/MPa	Tensile strength/ MPa	Young's modulus/ GPa	Poisson ratio	Cohesion c/MPa	Internal friction angle φ/°	Density /kg*m^{-3}
Andalusite schist	102.6	11.9	26.9	0.17	9.8	57.4	2810
Pre-calculated model rock	0.36	0.042	0.094	0.17	0.034	57.4	1870
Prepared model rock	0.35	0.107	0.103	0.16	0.53	21.6	1920

UCS of andalusite schist is the maximum value (load normal to foliation)

Figs 6.7.1 to 6.7.3 show the general model set-up including the monitoring systems, which consist of three main components:

- Strain gauge chains (deformation measurements)
- Infrared camera (high resolution temperature measurements)
- Digital speckle displacement field measurements (DIC = Digital Image Correlation)

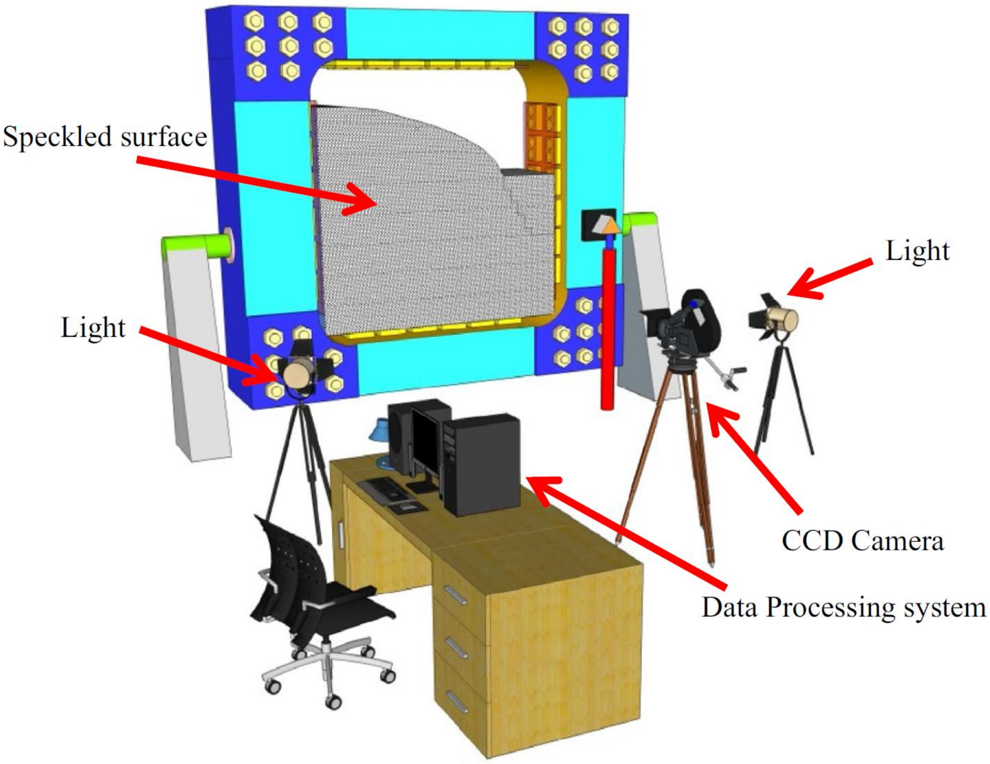

Fig. 6.7.1: Physical model set-up with DIC-system (Zhu et al. 2020)

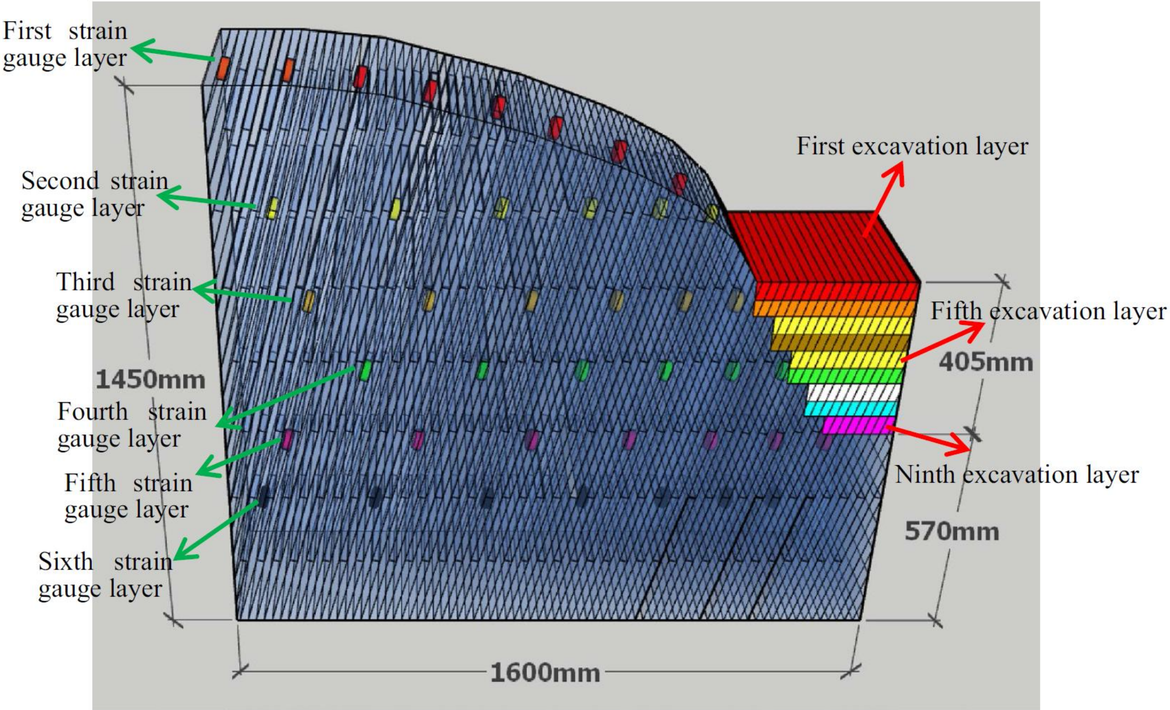

Fig. 6.7.2: Illustration of strain gauge layers in the physical model (coloured excavation layers are removed step-by-step to simulate the mining process) (Zhu et al. 2020)

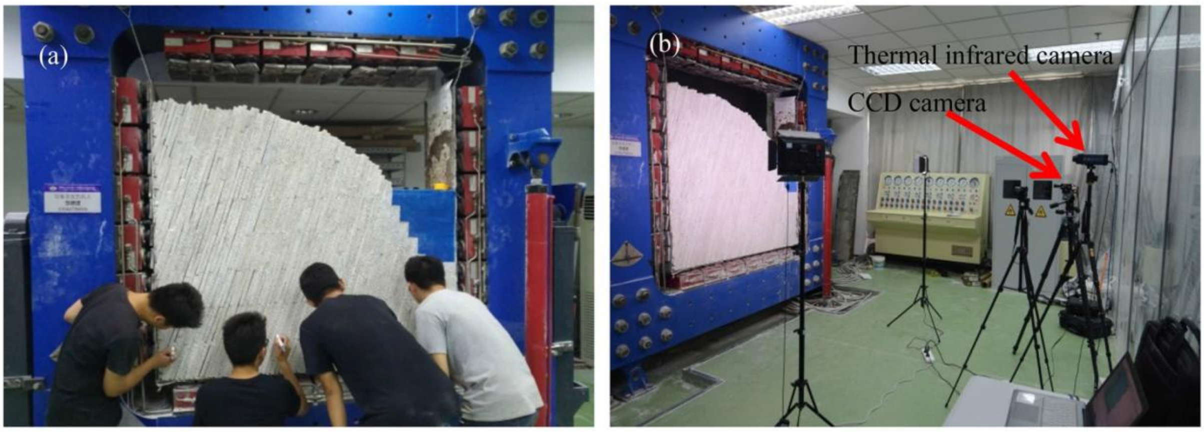

Fig. 6.7.3: Fotos of physical model incl. installed monitoring system (Zhu et al. 2020)

Figs 6.7.4 to 6.7.6 show model results in terms of failure pattern, temperature evolution and displacements triggered by simulating the open-pit mining process. Zhu et al. (2020) show, that the features observed in the physical model well duplicate the in-situ observations.

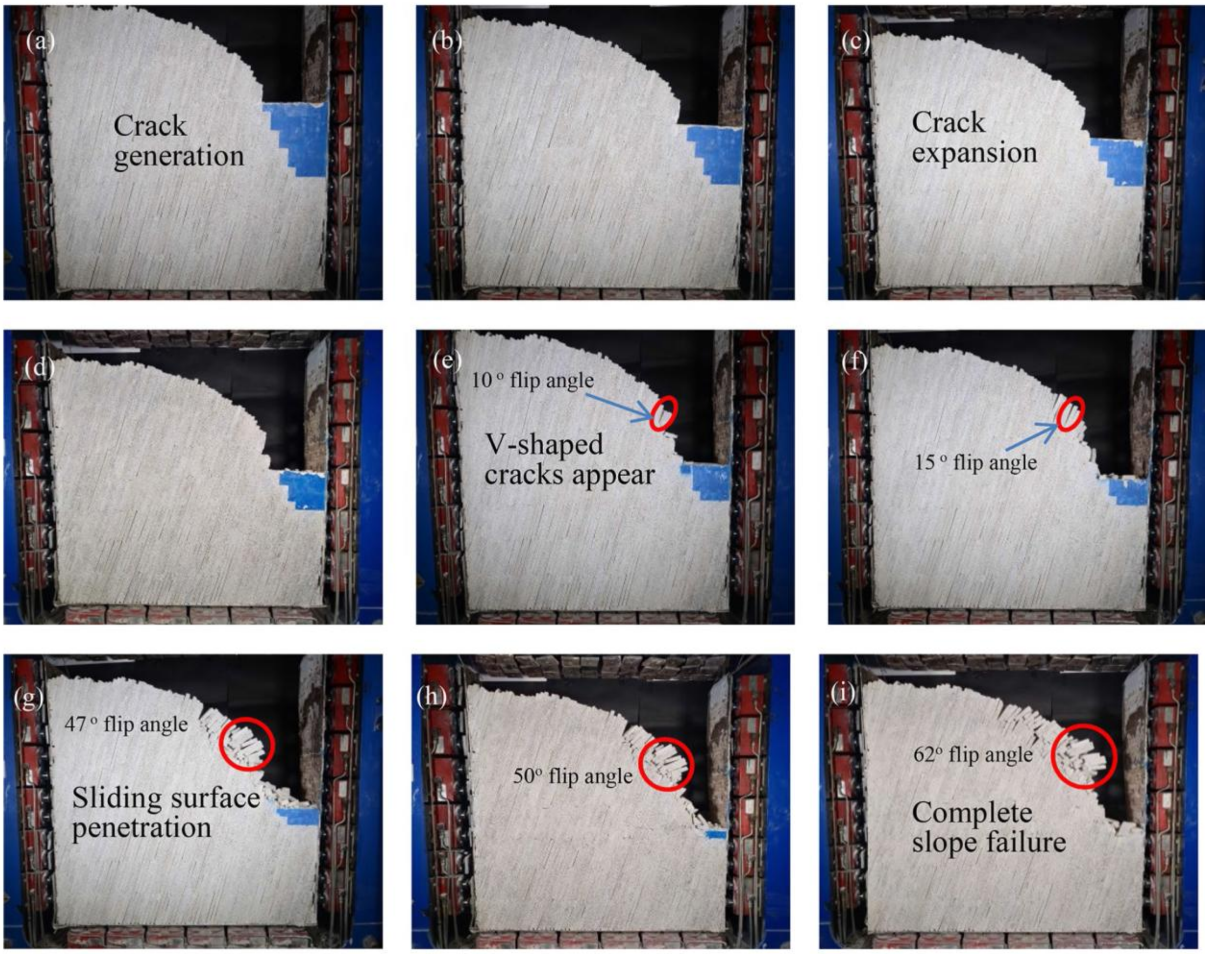

Fig. 6.7.4: Mining induced slope failure due to simulation of mining activity (stepwise removal of blue coloured layers)

Fig. 6.7.5: Detailed view of slope failure mechanism (toppling)

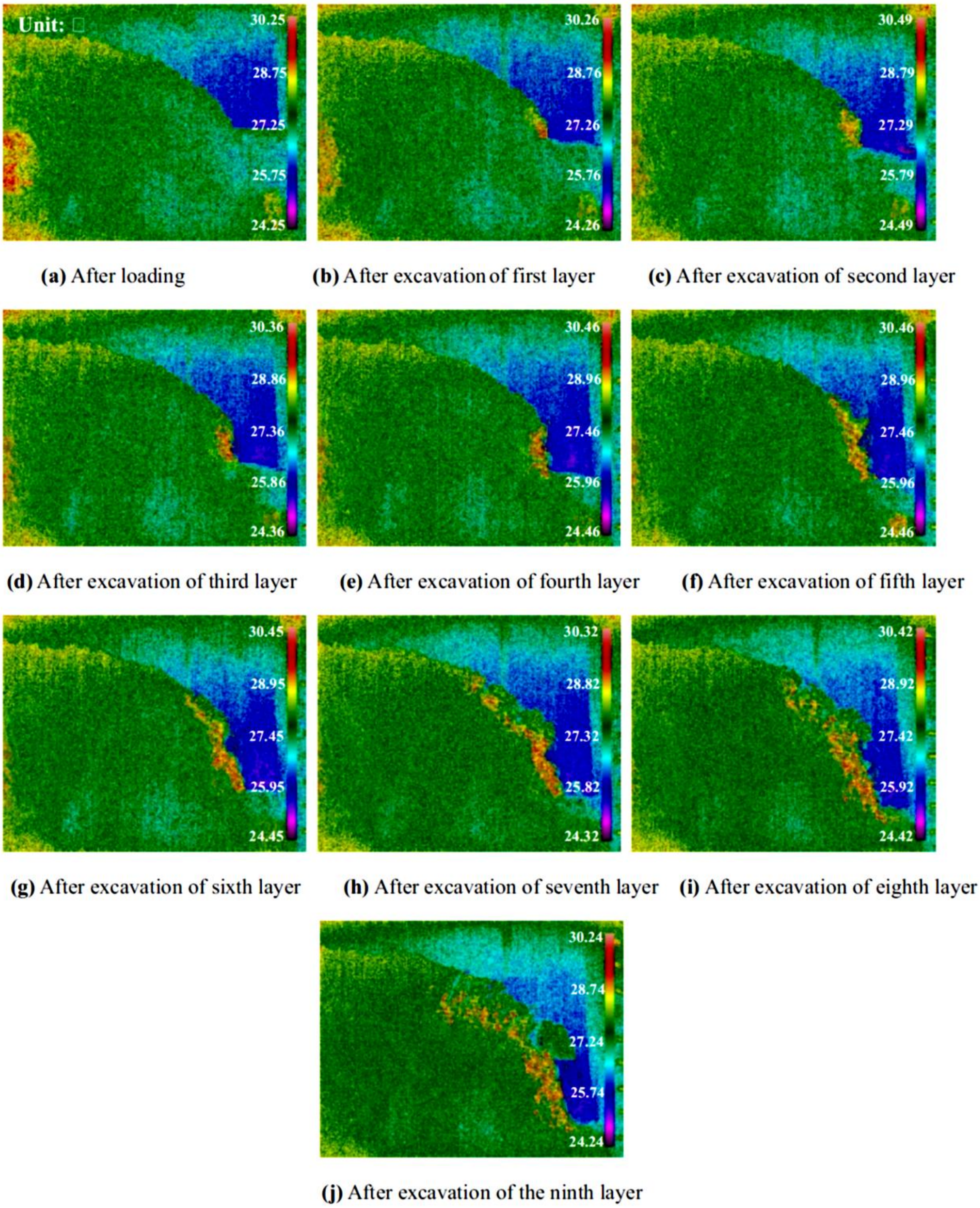

Fig. 6.7.6: Temperature evolution deduced from infrared camera observations during the simulated mining process (Zhu et al. 2020)

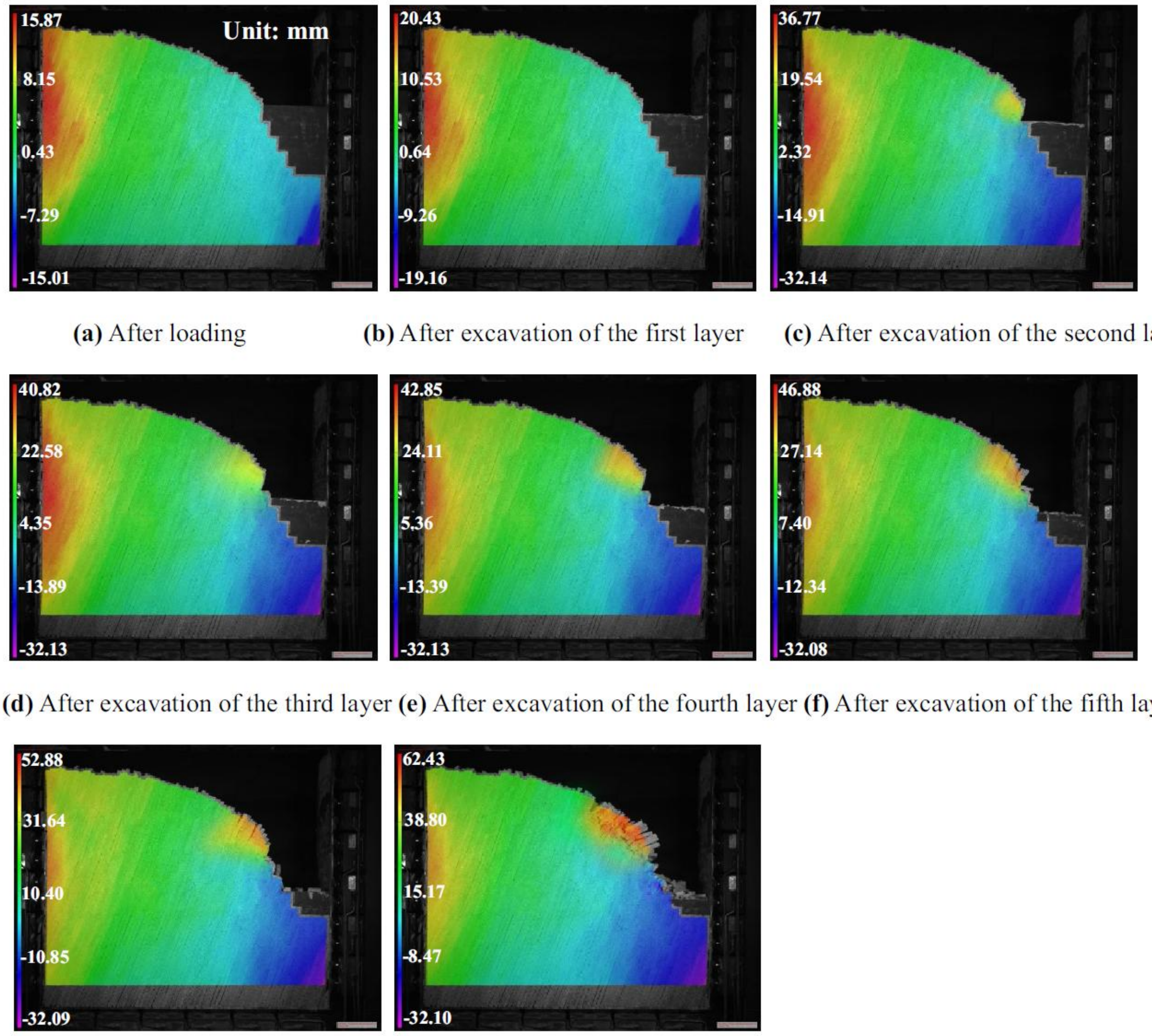

(a) After loading **(b)** After excavation of the first layer **(c)** After excavation of the second layer

(d) After excavation of the third layer **(e)** After excavation of the fourth layer **(f)** After excavation of the fifth layer

(g) After excavation of the sixth layer **(h)** After excavation of the seventh layer

Fig. 6.7.7: Evolution of horizontal displacement component obtained from DIC measurements

7 References

Al Heib, M.; Emeriault, F.; Caudron, M.; Nghiem, L. & Hor, B. (2013): Large-scale soil-structure physical model (1g) – assessment of structure damage, Int. Journal of Physical Modelling in Geotechnics, 13(4): 138-152

Bakhtar, K. (2000): Performance assessment of underground munitions storage facilities, *IJRMM Sci.*, 37(1-2): 369-384

Cheng, J.; Liu, F. & Li, S. (2017): Model for the prediction of subsurface strata movement due to underground mining, *J. of Geophysics and Engineering*, 14(6): 1608-1623

Gibbings, J.C. (2011): Dimensional Analysis, Springer, 295 p.

Hutter, K. (2014): Dimensional analysis, similitude and model experiments, in: *Physics of Lakes*, Springer, Vol. 3: 307- 396

Imre, B.; Laue, J. & Springman, S.M. (2010): Fractal fragmentation or rocks within sturzstrom: insight derived from physical experiments within the ETH geotechnical drum centrifuge, *Granular Matter*, 12: 267-285

Jacobi, O. (1976): Praxis der Gebirgsbeherrschung, Verlag Glückauf Essen, 496 p.

Jamei, M.; Hamrouni, F. & Trabelsi, H. (2017): Application of the hydraulic gradient method for physical modeling of rainfall induced landslide: the optimal design for a physical laboratory model, *Proc. JTC1 Workshop on Advances in Landslide Understanding,* Barcelona, Spain.

Li, Y.; Wang, H.; Zhu, W.; Li, S. & Li, J. (2015): Structural stability monitoring of a physical model test on an underground cavern group during deep excavations using FBG sensors, *Sensors*, 15: 21696-21709

Li, Z.; Liu, H.; Dai, R. & Su, X. (2005): Application of numerical analysis principles and key technology for high fidelity simulation to 3D physical model tests for underground caverns, *Tunneling and Underground Space Technology*, 20(4): 390-399

Li, Z. et al. (2010): Development and application of fluid-solid coupling similar materials in discharge test of old goaf water, *Geofluids*, ID 8834885

Liu, J.; Feng, X.-T.; Ding, X.-L.; Zhang, J. & Yue, D.-M. (2003): Stability assessment of the Three-Gorge dam foundation, china, using physical and numerical modeling – Part I: physical model tests, *IJRMM Sci,* 40(5): 609-631

Lirola, J.M.; Castaneda, E.; Lauret, B. & Khayet, M. (2017): A review on experimental research using scaled models for buildings: application and methodologies, *Energy and Buildings*, 142: 72-110

Mei, C.; Fang, Q.; Luo, H.; Yin, J. & Fu, X. (2017): A synthetic material to simulate soft rocks and its application for model studies of socketed piles, *Advances in Material Sciences and Engineering*, ID 1565438, 8 pages

Moosavi, M.; Karimi, A. & Yoosefi, M. (2009): A review on physical modeling in geomechanics, *Proc. SINOROCK-2009*, Hongkong, 5 p.

Ning, Z. et al. (2025): Application of physical model test in underground engineering: A review of methods and technologies, Transportation Geotechnics, doi.org/10.1016/j.trgeo.2025.101594

Obert, L. & Duvall, W.I. (1967): Rock mechanics and the design of structures in rock, John Wiley & Sons, 650 p.

Qiu, J. et al. (2021): Physical model test on the deformation behaviour of an underground tunnel under blasting disturbance, *Rock Mechanics Rock Engineering*, 54: 91-108

Sharma, R.H.; Konietzky, H. & Kosugi, K. (2010): Numerical analysis of soil pipe effects on hillslope water dynamics, *ActaGeotechnica*, 5: 33-42

Sharma, R.H. & Konietzky, H. (2011): Instumented failure of hillslope models with soil pipes, *Geomorphology*, 130: 272-279

Song, L.; Jiang, Q.; Shi, Y.-E.; Feng, X.-T.; Li, Y.; Su, F. & Liu, C. (2018): Feasibility investigation of 3D printing technology for geotechnical physical models: study of tunnels, *Rock Mechanics Rock Engineering*, 51: 2617-2637

Zhou, N.; Zhang, J.; Yan, H. & Li, M. (2017): Deformation behavior of hard roofs in solid backfill coal mining using physical models, *Energies*, 10(4): 10040557

Zhu, C et al. (2020): Investigating toppling failure mechanism of anti-dip layered slope due to excavation by physical modelling, *Rock Mechanics Rock Engineering*, 53: 5029-5050